

How ocean waves rock the Earth:

two mechanisms explain microseisms with periods 3 to 300 s

Fabrice Ardhuin^{1,2}, Lucia Gualtieri³, Eleonore Stutzmann³

¹Ifremer, Laboratoire d'Océanographie Spatiale, Brest, France.

²Laboratoire de Physique des Océans, CNRS-Ifremer-UBO-IRD, Brest, France

³Institut de Physique du Globe, PRES Sorbonne Paris-Cité, Paris, France.

Contents of this file

Text S1
Figures S1 to S4

Additional Supporting Information (Files uploaded separately)

none

Introduction

The text S1 gives more details and some corrections on the theory by Hasselmann (1963) as well as the practical implementation. The four figures illustrate various aspects related to the expected seismic sources on realistic bathymetric profiles.

Text S1.

Detailed theoretical aspects of the generation of seismic waves by ocean waves

We give here a few important details and corrections to the general theory laid out by Hasselmann [1963], with a particular attention to its application for long ocean waves with periods larger than 30 s. Both primary and secondary mechanisms enable the short surface gravity waves to generate much longer wavelengths, and thus much faster waves that can couple to seismic waves. The question we address is rather quantitative: how much seismic energy is radiated by each of these mechanism?

After giving the expression for transforming the wave-induced pressure into seismic ground displacement, which is common to both mechanisms, we detail the expressions of the long-wavelength pressure spectrum as a function of the usual ocean wave spectrum, beginning with the secondary mechanism because this is the most studied mechanism. This follows the plan of Hasselmann [1963], with less mathematical detail for some parts, and a final expression in terms of ocean wave spectra, as given by usual numerical models.

For both mechanisms the conversion of pressure in the ocean to seismic amplitudes uses the coupling coefficients that were first determined by Longuet-Higgins [1950, his figure 2], and recomputed by Gualtieri et al. [2013] using normal modes. This follows exactly what has been done for the secondary mechanism by Kedar et al. [2008], Ardhuin et al. [2011], Stutzmann et al. [2012] and others. In the case of the primary mechanism we apply the same formulation to the wave-induced pressure at the bottom because of the shallow water depth. Hence the oscillating bottom elevation is transformed into a flat bottom with a pressure at the sea surface.

1) From the wave-induced pressure spectrum at large wavelengths to seismic waves

For both primary and secondary mechanisms, the source of seismic waves S is a function of the wave-induced pressure spectrum at seismic wavelengths. Since these wavelengths are much larger than those of surface gravity waves, we may practically estimate the pressure spectral density at near-zero wavenumber. For linear waves in a homogeneous ocean (i.e. constant depth and current velocity), this spectral density would be zero. Its non-zero value is due to either nonlinearity (secondary mechanism) or spatial non-

homogeneity (primary mechanism). For a solid half space of density ρ_s and shear wave speed β , Longuet-Higgins [1950] and Hasselmann [1963] give the local seismic source as a function of the seismic frequency f_s and of the wave-induced pressure spectral density near zero wavenumber $F_p(k_x \approx 0, k_y \approx 0, f_s)$,

$$S(f_s) = 4\pi^2 f_s c^2 F_p(k_x \approx 0, k_y \approx 0, f_s) / (\beta^5 \rho_s^2) \quad (S1)$$

where c is a non-dimensional coefficient for microseismic generation [Longuet-Higgins 1950; Ardhuin and Herbers 2013], which is $c=0.2$ for $\beta=2.2$ km/s, $\rho_s = 2.6$ kg/m³, $\rho_w = 1.0$ kg/m³, and $T=200$ s with a water depth of 2000 m. The following sections give the details on how to compute F_p , based on the secondary mechanism considering $F_{p,2}$ (eq. S5) or based on the primary mechanism considering $F_{p,1}$ (eq. S22).

The pressure spectrum in eq. (S1) corresponds to the wave-induced spectrum at the sea surface. However, in the case of the primary mechanism, the water depth at the source is small compared to the acoustic wavelength and the bottom pressure is equivalent to a surface pressure.

This source S has S.I. units of m/Hz. Here we integrate these sources along great circle paths for all azimuths ϕ , and all epicentral distances Δ , taking into account the seismic attenuation and geometrical spreading [e.g. eq. (4.36) in Ardhuin and Herbers 2013]. The integral over Δ goes from zero to 2π , covering one full orbit around the Earth in each direction. The power spectral density of the seismic displacement is

$$F_\delta(f_s) = \int_0^{2\pi} \int_0^{2\pi} S(\Delta, \phi, f_s) \frac{\exp(-2\pi f_s \Delta R_E / UQ)}{(1-b) R_E \sin \Delta} R_E^2 \sin \Delta d\Delta d\phi, \quad (S2)$$

where b is the attenuation over one orbit around the Earth,

$b = \exp(-2\pi f_s 2\pi R_E / UQ)$, hence the factor $1/(1-b) = 1+b+b^2+b^3\dots$ corresponds to the incoherent sum of the energies of all the orbits. This incoherent sum for epicentric distances larger than one orbit is consistent with the coarse spectral resolution used in figure 2, in which the normal mode structure is not resolved. For spectra with frequency resolution finer than $U / (2\pi R_E)$ [e.g. Webb 2007], one could first perform a coherent sum over the orbits. Values of U and Q are discussed in the article and illustrated in figure S1.

A simple estimation of the shape and order of magnitude of the expected microseismic response to the ocean wave forcing in any water depth is provided by assuming a uniform source distribution S . In this case S reduces to a function of the seismic frequency f_s only. Under these assumptions the frequency spectrum of ground vertical displacement F_δ is uniform, and eq. (S2) writes,

$$F_{\delta}(f_s) = S(f_s) \int_0^{2\pi} \frac{\exp(-2\pi f_s \Delta R_E / UQ)}{(1-b)R_E \sin \Delta} R_E^2 2\pi \sin \Delta d\Delta = S U Q / f_s (1-b), \quad (S3)$$

where U is the group speed of the considered seismic mode, Δ is the epicentric distance between the source and the seismic station, R_E is the radius of the Earth and Q is the non-dimensional seismic attenuation factor.

Eq. (S3) is strictly valid for underwater measurements, within a region of homogeneous sea state. This was shown by Ardhuin et al. [2013] to apply for microseisms with periods of 3 s and less. For the general case of a variable sea state, we expect this equality to hold only for time and spatial averages. Since the measurements discussed here are generally made on land, and the oceans only cover part of the Earth surface, eq. (S3) is only expected to provide a reasonable order of magnitude. This approach is consistent the analysis in Webb [2007]. In this context we may neglect the $(1-b)$ factor, with $b = 0.35$ at 3 mHz, decreasing rapidly towards higher frequencies, with $b=0.01$ at 7 mHz.

Combining (S1) and (S3), for either the primary or secondary mechanism, we thus note that the seismic displacement power spectrum F_{δ} is directly proportional to the wave-induced pressure power spectrum F_p , and the f_s term in (S1) cancels the $1/f_s$ in (S3). This will be important for the asymptotic shapes of the seismic acceleration power spectrum for the primary and secondary mechanisms.

2) How short ocean waves make long seismic waves: Secondary mechanism

The seismic noise source given by the secondary mechanism is proportional to the square of the wave-induced orbital velocity at the sea surface [eq. 2.11 in ref Hasselmann 1963]. As a result, any pair of wave trains with velocities given by $u_1 \cos(k_1 x - 2\pi f_1 t)$ and $u_2 \cos(k_2 x - 2\pi f_2 t)$ will yield a surface pressure pattern that contain the term

$$u_1 u_2 \{ \cos[(k_1 + k_2)x - 2\pi(f_1 + f_2)t] + \cos[(k_1 - k_2)x - 2\pi(f_1 - f_2)t] \}. \quad (S4)$$

This nonlinear interaction of waves involves sum and difference interactions, which are given by the two parts of this interaction term.

2.a) Why the difference interaction of ocean waves cannot produce seismic waves in a horizontally homogeneous environment.

It is well known that difference interactions, the second part of eq. (S4) with the frequency $(f_1 - f_2)$ can have very long periods. Recent publications by Uchiyama and McWilliams [2008] and Traer and Gerstoft [2014] have used that result to suggest this interaction could directly generate seismic noise in the hum frequency band. However, only sum interactions, the first part of eq. (S4) with $(f_1 + f_2)$, were considered for seismic wave generation theory. The reason for neglecting difference interactions, is that they cannot produce fast traveling waves in a horizontally homogeneous environment. This was already mentioned by Hasselmann [1963], and discussed in Webb [2008].

Namely, the difference interactions cannot match the wavenumbers of seismic

components. This is clearly established by considering any pair of frequencies f_1 and f_2 , with $f_2 > f_1$. The speed $C_2 = 2\pi(f_2 - f_1)/|\mathbf{k}_2 - \mathbf{k}_1|$ is fastest for \mathbf{k}_1 and \mathbf{k}_2 aligned and in the same direction. For a constant depth D , these frequencies f_i are functions of the norms k_i of \mathbf{k}_i given by the linear dispersion relation $f_i = h(k_i) = g k_i \tanh(k_i D)/(2\pi)$, where g is the acceleration of gravity. Applying the Taylor-Lagrange formula, there is a wavenumber k_3 such that

$$[f_2 - f_1]/(k_2 - k_1) = h'(k_1) + (k_2 - k_1)h''(k_3)/2.$$

The group speed of ocean waves is $2\pi h'(k_1)$, known to be slower than the ocean phase speed. Because $h''(k)$ is strictly negative, then C_2 is less than this ocean phase speed, itself much slower than the seismic waves.

2.b) Surface and bottom pressure induced by sum interactions

Ocean wave properties are usually represented by a wave frequency-directional spectrum $E(f, \theta)$, where f is the wave frequency, and θ is the azimuth of ocean waves. Only the direction-integrated spectrum $E(f)$ is really well known,

$$E(f) = \int_0^{2\pi} E(f, \theta) d\theta.$$

Very few estimates [Ardhuin et al., 2012; Ardhuin et al. 2013] are available for the directional “overlap integral”, defined here using the convention of Webb [2008], which is twice the value used in Ardhuin and Herbers [2013],

$$I(f) = \int_0^{2\pi} E(f, \theta) E(f, \theta + \pi) d\theta / E^2(f).$$

In deep water, the spectral density at $k_x = k_y = 0$ of the equivalent second order pressure at the sea surface that generates seismo-acoustic noise is given by Hasselmann [1963] and Ardhuin and Herbers [2013],

$$F_{p,2}(k_x = 0, k_y = 0, f_s) = (\rho_w g)^2 f E^2(f) I(f) \quad (S5)$$

where $f_s = 2f$ is the seismic frequency, equal to twice the ocean wave frequency f , g is the acceleration of gravity and ρ_w is the water density.

Finite depth effect in the secondary mechanism

Because we are also dealing with very long waves that also modify directly the bottom pressure, we need to consider the effect of wave-induced bottom pressure together with the wave-induced pressure at the sea surface. That additional bottom pressure term was not considered in previous investigations on the hum by Webb [2007, 2008].

On the full model grid we compute the second order pressure spectrum at the sea surface and at near-zero seismic wavenumber k_s . This is given by eq. (2.29) in Ardhuin and Herbers [2013]. Ardhuin and Herbers [2013] showed that considering the wave-induced pressure at the ocean bottom gives a reduction by a factor

$$G(kD) = [\tanh(kD)]^2 [1 + 2kD/\sinh(2kD)], \quad (S6)$$

where the ocean wavenumber k is related to the wave frequency f by the linear wave

dispersion relation

$$(2 \pi f)^2 = gk \tanh(kD),$$

with D the water depth. For long periods and shallow water, $kD \ll 1$, and $G(kD)$ can be replaced by $2 \tanh^2(kD)$. In practice, this correction has no significant effect for seismic waves with periods around 5s, for which most of the sources are in deep enough water for the approximation $G \approx 1$ to be accurate as used by Stutzmann et al. [2012], but it changes the results for the hum by several orders of magnitude.

Because the orbital velocities induced by ocean waves are much larger for a given height when waves are in shallow water, it was expected by Webb [2007] that microseismic sources would be amplified compared to deep water. Instead, the reduction in bottom pressure is fundamentally related to the Bernoulli effect, in which the pressure drops proportionally to the square of the velocity. Applied at the bottom and in the limit $kD \rightarrow 0$, this effect exactly cancels the surface velocity effect. This cancellation is a well known property in the incompressible context [Herbers et al. 1991; Ardhuin and Herbers 2013] and is supported by bottom pressure observations that resolve both the short and long ocean waves [Herbers et al. 1991]. The consistency between the compressible and incompressible theories is detailed in the appendix A of Ardhuin and Herbers [2013], with the sum of surface and bottom contributions given there by eq. (A4).

Power law behavior of wave and microseismic spectra for the secondary mechanism

Combining eqs. (S1), (S3) and (S5) gives a dependence of the vertical displacement power spectrum on the seismic frequency that is proportional to f_s if $E(f, \theta)$ is constant, giving a power spectrum of the acceleration proportional to f_s^5 . In our model, $E(f, \theta)$ increases like f_s around $f_s = 10$ mHz. That increase and the factor $G(kD)$ combine to give an acceleration power spectrum that is closer to f_s^8 . At higher wave frequencies $f = 0.15$ Hz, the wave spectrum typical decreases like f^{-n} with n between 4 and 5. Taking $n=4$ gives the observed shape of the acceleration power spectrum, decreasing like $f_s^{4+1-2n} = f_s^{-3}$ (Figure 2a).

3) How short ocean waves make long seismic waves: Primary mechanism

This mechanism is a linear transformation of ocean waves into seismic waves of the same frequency f . For a practical application we use the wave model output of $E(f, \theta)$ along shorelines, and more particularly its value in the direction perpendicular to shore. The primary mechanism was previously explored in the case of constant bottom slopes by Hasselmann [1963]. We give here a few more details and show general results for realistic bottom profiles. We estimate the spectral density at $k_x = k_y = 0$ in order to give, for the primary mechanism, the equivalent of the secondary source of eq. (S5).

We estimate a similar pressure spectrum at large wavelengths, for the first order pressure field in the presence of a sloping bottom. The final result is eq. (S22). We first characterize the bottom pressure field for a monochromatic wave train, and then apply that result to random waves and express the pressure spectrum as a function of the wave spectrum $E(f, \theta)$.

3.a) Bottom pressure for monochromatic waves

A monochromatic wave train propagating over depths varying only in direction x gives field of surface elevation and bottom pressures, with amplitudes that are modulated as shown in figure 1.c. In order to normalize all the wave-related fields, we use the wave amplitude a_A for a reference depth that we set at $D_A = 4000$ m. The assumption of alongshore uniformity is appropriate if the depth varies alongshore on scales much larger than the seismic wavelength. For cases where the depth varies in the y direction at scales comparable or shorter than the seismic wavelength, we only expect a qualitative agreement, which is supported by preliminary tests with a phase-resolving refraction-diffraction model. We note that for linear ocean waves over a flat bottom, the dispersion relation is

$$(2 \pi f)^2 = gk \tanh(kD), \quad (S7)$$

where k is the wavenumber, f is the frequency, D is the water depth, and g is the vertical acceleration due to gravity.

We will see that one effect of the bottom slopes is to put a very small fraction of the ocean wave energy at wavenumbers that are very far from this linear dispersion relation. With an alongshore wavenumber k_y we consider the bottom pressure $P_0(x, k_y, f)$ induced by our monochromatic wave train, normalized by the wave amplitude a_A . Because of this normalization, P_0 has units of Pa/m. Its Fourier transform in the x dimension over a distance L_x is

$$K(f, k_x, k_y) = \frac{1}{2\pi} \int_{-L_x}^0 P_0(x, k_y, f) e^{ik_x x} dx,$$

(S8) which has units of Pa. This spectrum K is used with the same definition by Hasselmann [1963]. The actual bottom pressure spectrum is $a_A K$, with units of Pa.m. In Hasselmann, the eq. (4.23) is an integral from minus infinity to plus infinity. Here we have defined our Fourier transforms over a finite domain because this is how it is used for practical applications in the next section. Because the shoreline is at $x=0$, P_0 is zero for $x > 0$. As a result our definition of K is the same as Hasselmann's, in the limit $L_x \rightarrow \infty$. Figure S2 shows examples of the pressure field at the bottom for waves propagating in one dimension.

If k_y is smaller than the magnitude of seismic Rayleigh wavenumbers, then the broad spectrum of K overlaps with wavenumbers of seismic Rayleigh waves. In practice the spectrum K is nearly white, i.e. weakly dependent on wavenumbers near $k_x = k_y = 0$. We can thus replace K by its value at $k_x = 0$, which corresponds to the x -average of the pressure signal, and $k_y = 0$, which corresponds to waves exactly perpendicular to the depth contours.

The alongshore wavenumber k_y is the same for ocean and seismic waves, and is unchanged during cross-shore propagation. Since we are considering only the spectral components of the ocean wave field that can couple to seismic Rayleigh waves, with a typical phase speed $C_s = 3$ km/s, the ocean waves must have propagation angles that are nearly perpendicular to the depth contours, namely the ratio of the alongshore wavenumber k_y to the wavenumber magnitude k should be less than the ratio of the ocean wave to seismic wave phase speeds C / C_s , which is always less than 0.1.

3.b) Theoretical expression for the pressure spectrum

The bottom pressure power spectral density is, by definition, the ratio of the bottom pressure variance and the spectral increment,

$$F_{p,1}(f, k_x, k_y) = \frac{|a_A K(k_x, k_y, f) \Delta k_x|^2}{\Delta k_x \Delta k_y \Delta f}. \quad (\text{S9})$$

Mathematically, eq. (S9) is correct in the limit of small spectral increments, which correspond to spectra estimated over long times and distances. In practice, due to the spatial inhomogeneities and temporal variability of the sea state, we estimate (S9) with finite spectral increments $\Delta k_x = 2\pi/L_x$, $\Delta k_y = 2\pi/L_y$, $\Delta f = 1/\tau$, where L_x , L_y , and τ are the lengths over which the Fourier transform is computed in the three dimensions. The definition of the wave directional spectral density is again the ratio of the variance (this time of the surface elevation) divided by the spectral increment,

$$E_A(f, k_y) = \frac{|a_A|^2}{\Delta k_y \Delta f}. \quad (\text{S10})$$

We now change the spectral coordinates ($f, k_y = k \sin \theta$) to the more usual (f, θ) where θ is the azimuth of the ocean waves. The Jacobian of this spectral coordinate transform is $k \cos \theta$. For $\theta=0$, $\cos \theta=1$ and eq. (S10) gives

$$E_A(f, \theta=0) = k_A E_A(f, k_y=0), \quad (\text{S11})$$

where, at location A, the depth is D_A , and the norm of the wavenumber vector is k_A , as given by eq. (S7), namely $(2\pi f)^2 = g k_A \tanh(k_A D_A)$.

We can now replace the wave amplitude a_A in eq. (S9) by the wave spectrum (S11), using (S10), and we arrive at the first order bottom pressure spectrum. We particularly consider the power spectral density relevant for seismic wave generation, with $k_x = 0$, $k_y = 0$,

$$F_{p,1}(k_x=0, k_y=0, f) = \frac{E_A(f, \theta=0)}{k_A} |K^2(k_x=0, k_y=0, f)| \frac{2\pi}{L_x}. \quad (\text{S12})$$

This expression is inversely proportional to L_x , the length over which the spectrum is evaluated. This is so because the relevant pressure perturbation is localized at a scale much smaller than L_x .

For an alongshore distance L_y , and a frequency bandwidth df the bottom pressure spectrum given by (S12) is equivalent, for small k , to the one produced by a vertical force oscillating with a frequency f and an amplitude F [Hasselmann 1963, Gualtieri et al. 2013]. This amplitude is simply the area $L_x L_y$ multiplied by the square root of twice the corresponding pressure variance,

$$F = 2\pi \sqrt{2 L_x L_y F_{p,1}(k_x=0, k_y=0, f) df}. \quad (\text{S13})$$

Given (S12), this force F does not depend on L_x , and varies like the square root of L_y

which corresponds to an incoherent sum of sources in the y direction. For $k_x = 0, k_y = 0$, eq. (S8) becomes a spatial average

$$K(k_x=0, k_y=0, f) = \frac{1}{2\pi} \int_{-L_x}^0 P_0(x, k_y=0, f) dx. \quad (\text{S14})$$

The usual spectral density is obtained when the length L_x goes to infinity, but for practical estimates, this length is always finite. Without any wave dissipation, the pressure field at the bottom is given by the following equations. First the local group speed is defined from the local water depth D and the frequency f

$$C_g = \frac{2\pi f}{k} \left(0.5 + \frac{kD}{\sinh(2kD)} \right) \quad (\text{S15})$$

in which k is estimated from D and f using eq. (S6). The conservation of the energy flux gives the local surface elevation amplitude a ,

$$C_g a^2 = C_{gA} a_A^2. \quad (\text{S16})$$

The phase is obtained by integrating the local ocean wavenumber k , [e.g. Mei 1989],

$$S(x) = \int_0^x k(x') dx'. \quad (\text{S17})$$

These amplitudes and phase can be used to determine the surface elevation,

$$\zeta(x, k_y=0, f) = a_A \sqrt{\frac{C_g}{C_{gA}}} e^{iS}.$$

Using linear wave theory gives the conversion factor from surface elevation to the bottom pressure, which, divided by the amplitude a_A gives

$$P_0(x, k_y=0, f) = \frac{\rho_w g}{\cosh(kD)} \sqrt{\frac{C_g}{C_{gA}}} e^{iS}. \quad (\text{S18})$$

All this is enough to estimate the pressure spectrum defined by (S12). We have used this eq. (S18) to compute the pressure field over the bottom, as shown by the red curve in figure 1.c.

3.c) Practical calculation

In general there is no simple expression for the pressure integral (S14). For a constant bottom slope D' , Hasselmann [1963] has evaluated (S14), and proposed that

$$|K|^2 = \frac{\rho_w^2 g^4}{(2\pi f)^4 64\pi} D'. \quad (\text{S19})$$

we will in particular use his value for $D' = 1\%$,

$$|K_1|^2 = \frac{0.01 \rho_w^2 g^4}{(2\pi f)^4 64\pi}. \quad (\text{S20})$$

We now revise this analytical expression, which is not exact but is still a good

approximation of (S14), for slopes D' between 1.5 and 4%. Near the shoreline, where $x=0$ and $S=0$, the integrand in (S14) is proportional to $\sqrt{S} e^{iS}$. Under the incorrect assumption that the integral of $\sqrt{S} e^{iS}$ from $S=0$ to infinity is defined, eq. (S19) was obtained by Hasselmann [1963] using contour integration on the complex plane [Hasselmann, personal communication 2013]. In practice, the integrand for large S is very different from $\sqrt{S} e^{iS}$ and goes to zero, which keeps the integral (S14) defined. For D' between 1.5 and 4% we found that (S19) is within 10% of our numerical estimates using the full expression for (S14). We also verified that (S8), with the non-zero wavenumber components k_x and k_y expected for Rayleigh waves, gives similar results.

We now consider any bottom depth profile, with the only assumption that the depth is constant in the y direction. To simplify the notations, we introduce a normalized seismic source s , using eqs. (S14) and (S20),

$$s = |K|^2 / |K_1|^2. \quad (\text{S21})$$

This parameter s contains all the effects of the bottom topography and is an ‘‘effective slope’’. s is a non-dimensional parameter that depends on the depth profile and the wave frequency f . We finally use a wave-induced pressure power spectrum expressed as follows,

$$F_{p,1}(k_x=0, k_y=0, f) = s \frac{E_A(f, \theta=0)}{k_A} \frac{\rho_w^2 g^4}{(2\pi f)^4 3200 L_x}.$$

This equation is directly used to compute seismic sources in figure 3, with the direction $\theta=0$ replaced by the local shore-normal direction θ_n , and, to take into account waves propagating towards the shore and away from the shore we replace $E(f, \theta=0)$ by $[E(f, \theta_n) + E(f, \theta_n + \pi)]$,

$$F_{p,1}(k_x=0, k_y=0, f) = s \frac{\rho_w^2 g^4 [E_A(f, \theta_n) + E_A(f, \theta_n + \pi)]}{k_A (2\pi f)^4 3200 L_x}. \quad (\text{S22})$$

Estimates of s for different bottom profiles are shown in Figure S3.

Eq. (S22) can be combined to eq. (S3) to estimate the shape of the seismic response. Taking A in 4000 m depth, then k_A is proportional to f for f smaller than 10 mHz. A constant spectrum E_A gives a pressure spectrum $F_{p,1}$ predicted by the primary mechanism that decreases like f^{-5} . Combined with eq. (S3) this gives a vertical displacement power spectrum that decreases like f^{-5} and an acceleration power spectrum that follows f^{-1} . Since our numerical model in the infragravity wave band actually predicts a spectrum E_A that grows like f from 5 to 15 mHz, this explains the nearly constant acceleration spectrum in that frequency range. At higher frequencies, a decrease of the wind wave spectrum like f^{-4} around $f=0.1$ Hz gives a f^{-5} seismic acceleration power spectrum.

3.d) Interpretation of the source dependence on the bottom profile

Eq. (S22) is interesting because it gives a practical expression for the pressure spectral density. However, the use of Fourier transforms removes the spatial resolution, and

prevents us from understanding which is the part of the depth profile that is responsible for the seismic source. In order to discuss spatial distribution of sources, we thus define a partial spatial integration $s(x)$,

$$s(x) = \frac{1}{(2\pi)^2 |K_1|^2} \left| \int_x^0 P_0(x', k_y, f) dx' \right|^2.$$

(S23)

Combining eqs. (S13) and (S20), this definition gives $s(-L_x) = s$, namely, the limit of $s(x)$ when reaching the end of the depth profile is the noise source previously defined. The quantity $s(x)$ is plotted in figures S1g and S1h. The locations where $s(x)$ varies most rapidly can be interpreted as the locations where the seismic sources are strongest.

3.e) Surf zone parameterization

An important detail for wave periods between 10 and 50 s is the treatment of the surf zone.

The ocean wave height decreases rapidly to zero for wave periods shorter than 30 s, and becomes roughly constant in the infragravity wave band. Hasselmann [1963] had proposed to represent the effect of wave dissipation in shallow water by an abrupt reduction of the bottom pressure to zero at a position x_b . Such a sharp jump in bottom pressure would give an order of magnitude increase of s . Instead, we prefer to reduce gradually the wave amplitude, and thus the bottom pressure, by a factor proportional to the water depth, giving the more realistic amplitude and pressure distribution shown in Fig. (S1.f). In the case of a smooth bottom topography, this treatment of the surf zone reduces s by one order of magnitude. Using a constant amplitude, more appropriate for the infragravity wave band (i.e. $T > 30$ s), did not significantly change the results.

3.f) Effects of unresolved bathymetric features

By taking into account realistic depth variations on the scale of the ocean wavelength for sandy bottoms, the value of s is typically increased by an order of magnitude, for periods in the range 10 to 30 s. Here we have used an empirical spectrum of the bottom elevation,

$$F_B(k_b) = 1.5 \times 10^{-4} k_b^{-3}, \quad (\text{S24})$$

which is consistent with depth soundings over sandy continental shelves [Hino 1968; Ardhuin and Magne 2002]. This impact of the depth oscillations, on the scale of the ocean wavelength, can be interpreted as a classical wave-wave interaction process [Hasselmann 1966] with the ocean waves of wavenumber vector k_1 coupling to bottom depth perturbations of wavenumber vector k_b to generate seismic waves of the same frequency but wavenumber $k_1 + k_b$.

In practice we have estimated the ratio $s = |K|^2/|K_1|^2$ for many different bottom profiles and wave periods. Our simple choice $s = 6$ is consistent with these calculations, within one order of magnitude (figures S2 and 2), and gives a reasonable fit to the measured hum, as shown in figures 2, 3 and 4. We have used east-west depth profiles at a 1 degree interval around 41° N [mid-Atlantic ridge, Lourenco et al. 1998], and 0.2° intervals around 46.47°N [Bay of Biscay, Anonymous 2008], 41.473°N [Oregon shelf, U.S. DoC NOAA/NGDC 2006], and north-south profiles around 157.8°W across the Oahu north

shore, Hawaii [Anonymous 2011].

3.g) Choice of s for our calculations

When evaluating the integral (S14) with the linear wave-induced bottom pressure (S18) we generally found a slightly larger value of s for frequencies below 10 mHz, with a maximum value obtained for the Hawaii bathymetry profile $s=40$ at 5 mHz. The fundamental reason why s is larger at these low frequencies, is that there are not strong enough slopes for depth such that $kD > 0.76$. Indeed, for $f=5$ mHz, $kD = 0.76$ corresponds to $D=4800$ m.

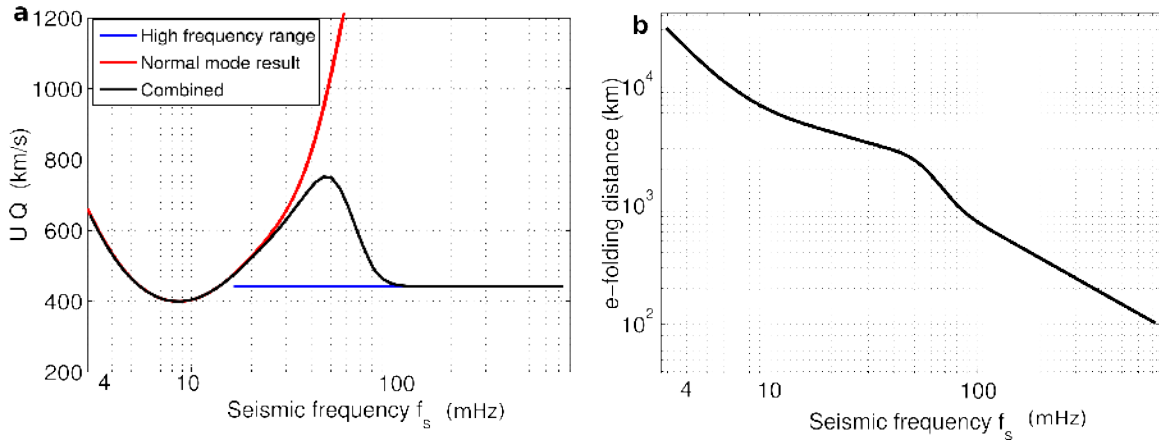
For short periods (typically less than 30 s), the value of s critically depends on the magnitude of the bottom depth perturbations at wavelengths similar to the ocean surface wavelength (around 100 m), and would otherwise be as low as 0.1 for a smooth bottom on these scales. The constant value $s = 6$, gives good results for the hum amplitude (Fig. 2). The good amplitude for the primary peak also should not be overstated. At these shorter periods we would expect s to be lower (figure S2) and we know that the seismic attenuation model is not well constrained. Finally we also expect that the alongshore variation in water depth lead to quantitative deviations from the previous result. This aspect has not been explored in the present paper.

References:

- Anonymous, A 500 m resolution bathymetry of the Bay of Biscay and Channel. <http://diffusion.shom.fr/produits/bathymetrie/mnt-golfe-de-gascogne-manche-500m.html> (2008).
- Anonymous, a 50 m resolution synthesis bathymetry and topography map of the Hawaiian islands, <http://www.soest.hawaii.edu/HMRG/multibeam/> (2011)
- Ardhuin, F., and Magne, R. Current effects on scattering of surface gravity waves by bottom topography. *J. Fluid Mech.*, **576**, 235 (2007).
- Ardhuin, F., Balanche, A., Stutzmann, E., and Obrebski, M.. From seismic noise to ocean wave parameters: General methods and validation, *J. Geophys. Res.* **117**, C05002 (2012).
- Ardhuin, F., and Herbers, T. H. C. Noise generation in the solid Earth, oceans and atmosphere, from nonlinear interacting surface gravity waves in finite depth. *J. Fluid Mech.*, **716**, 316-348 (2013).
- Ardhuin, F., Lavanant, T., Obrebski, M., Marié, L., Royer, J.-Y., d'Eu, J.-F., Howe, B. M., Lukas R., and Aucan, J. A numerical model for ocean ultra-low frequency noise: Wave-generated acoustic-gravity and Rayleigh modes. *J. Acoust. Soc. Am.* **134**, 3242–3259 (2013).
- Hasselmann, K. A statistical analysis of the generation of microseisms. *Rev. Geophys.*, **1**, 177 (1963).
- Hasselmann, K. Feynman diagrams and interaction rules of wave-wave scattering processes. *Rev. Geophys.*, **4**, 1 (1966).
- Herbers, T. H. C., Guza, R. T. Wind-wave nonlinearity observed at the sea floor. Part I: Forced-wave energy. *J. Phys. Oceanogr.*, **21**, 1740–1761 (1991).
- Gualtieri, L., Stutzmann, E., Capdeville, Y., Ardhuin, F., Schimmel, M., Mangeney, A., and Morelli, A. Modelling secondary microseismic noise by normal mode summation, *J. Int.*, **193**, 1732–1745 (2013).

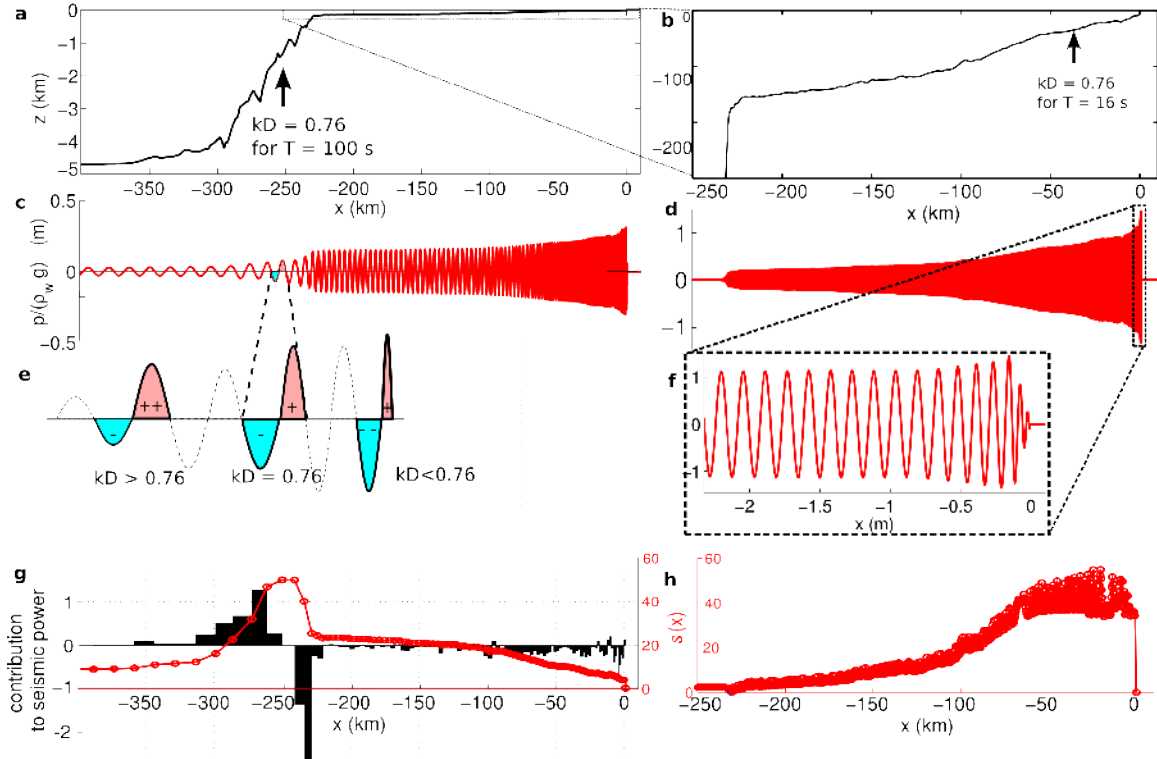
- Hino, M. Equilibrium-range spectra of sand waves formed by flowing water. *J. Fluid Mech.*, **34**, 565 (1968).
- Longuet-Higgins, M. S. A theory of the origin of microseisms. *Phil. Trans. Roy. Soc. London*, **A243**, 1–35 (1950).
- Lourenço, N. , Miranda, J.M., Luis, J.F., Ribeiro, A., Mendes Victor, L.A., Madeira, J., and Needham, H.D. Morpho-tectonic analysis of the Azores volcanic plateau from a new bathymetric compilation of the area, *Marine Geophysical Researches*, **20**,141-156 (1998).
- Mei, C. C. Applied dynamics of ocean surface waves. World Scientific, 2nd ed. (1989).
- Stutzmann, E., Arduin, F., Schimmel, M., Mangeney, A., and Patau, G. Modelling long-term seismic noise in various environments. *Geophys. J. Int.*, **191**, 707 – 722 (2012).
- U.S. Department of Commerce, National Oceanic and Atmospheric Administration, National Geophysical Data Center. *2-minute Gridded Global Relief Data (ETOPO2v2)*, (2006).

Figure S1.



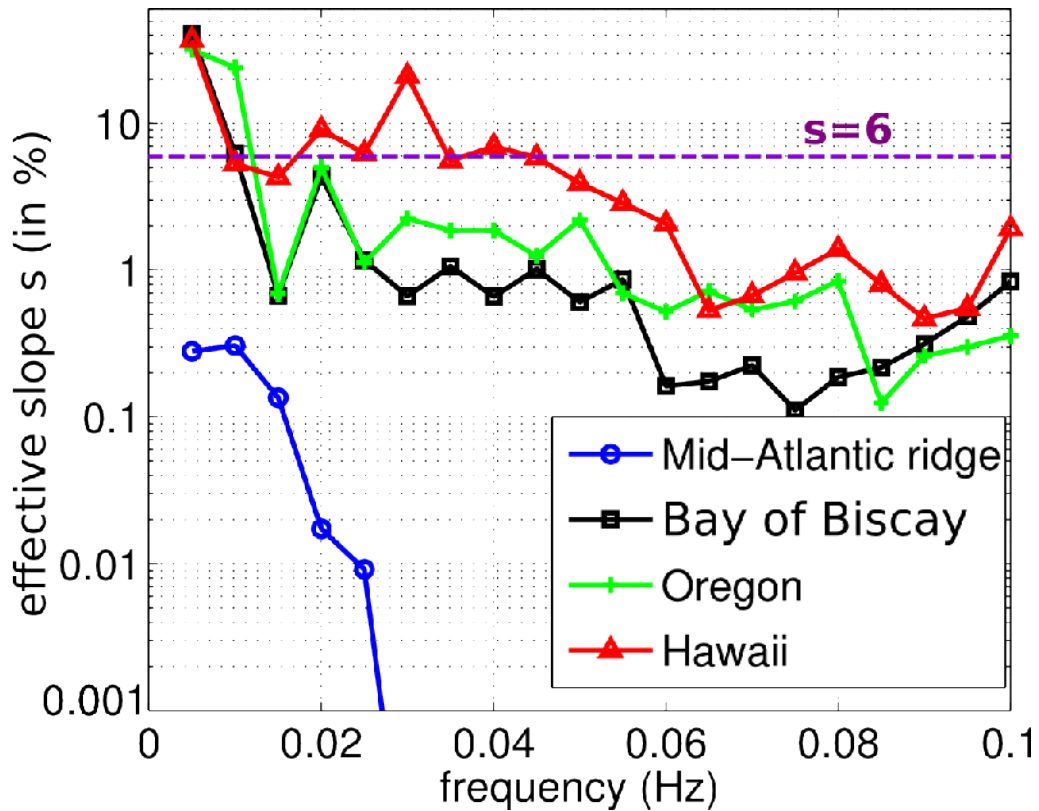
Supporting information, figure S1. Attenuation of seismic waves in our model. a, Values of UQ obtained by combining QL6 for Q and PREM for U (computed with a water depth of 2 km), for periods larger than 30 s with a constant $U=1.8$ km/s and $Q=240$ for shorter periods. **b,** Corresponding distance over which the seismic energy is reduced by a factor 2.7. For a period of 250 s ($f_s=4$ mHz) this distance is half-way round the globe, which allows the constructive interference that yields the modal structure seen in high-resolution spectra (e.g. Webb 2007).

Figure S2.



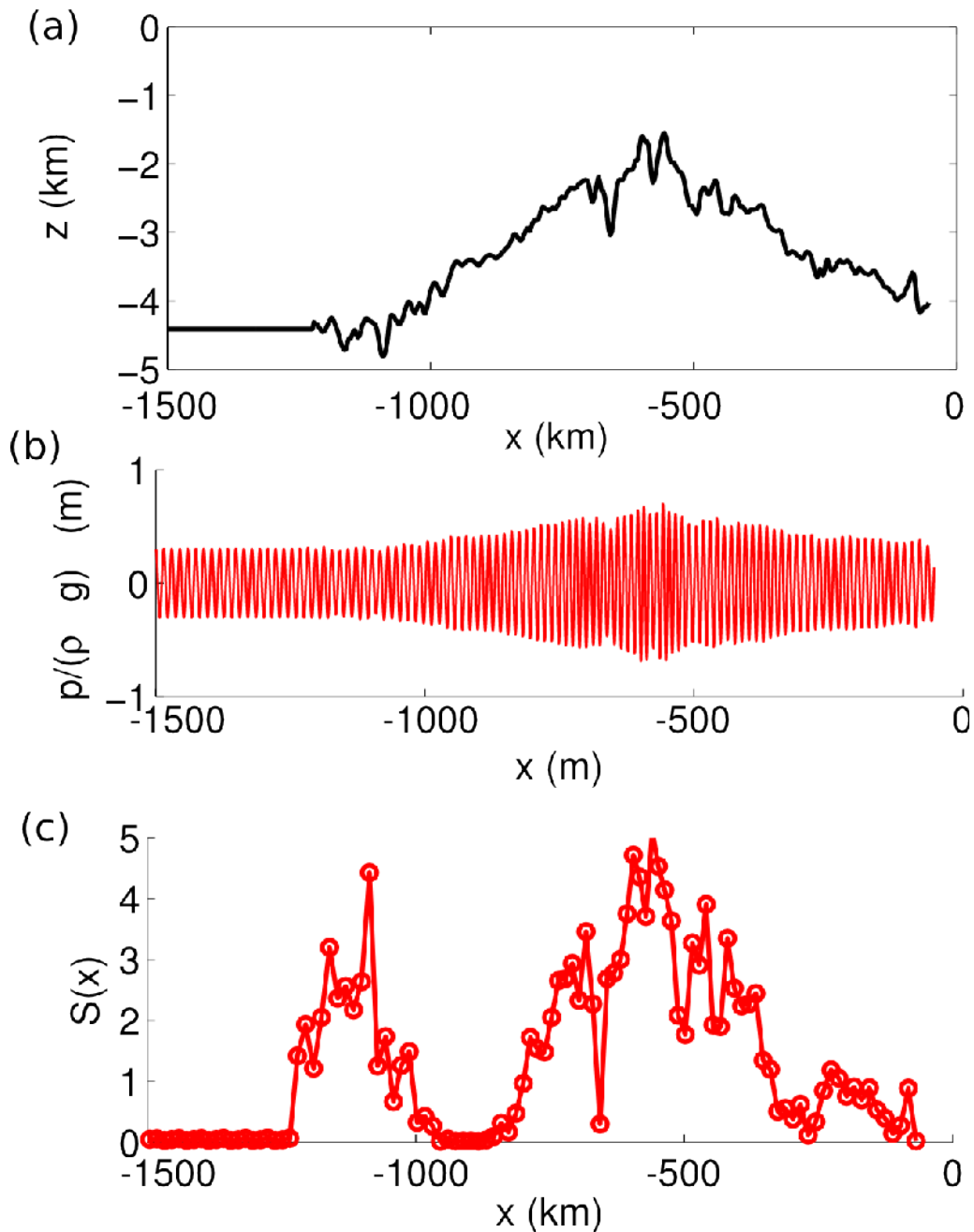
Supporting information, figure S2. How ocean waves propagating over a sloping bottom produce very long wavelength components capable of coupling to seismic Rayleigh waves. Example with waves of period 100 s and 16 s, over a continental shelf. **a,b** Example bottom topography in the Bay of Biscay at 47° N. **c** Snapshot of the bottom pressure computed using linear wave theory and energy conservation – except in the surf zone, for a period of 100 s and **d**, 16 s. **e**, Schematic showing how the pressure in a trough, with negative values, does not exactly cancel the pressure in the adjacent crest, due to a combination of wavelength shortening and increase in wave amplitude, giving a systematic phase shift between the wavelength-averaged pressure and the local pressure. For a non-dimensional depth $kD > 0.76$, corresponding to $x > 250$ km in **c,e,g**, the amplitude changes dominate. In shallower water the shortening dominates, giving opposing contributions to the mean pressure. **f**, close-up on the surf zone and reduction in wave amplitude due to breaking near the shore. **g,h**, In red, expected normalized seismic source power $s(x)$ due to waves between the shoreline and the local position x as defined in eq. (S22). In **g** the areas of black bars are proportional to the increment in source power over one ocean wavelength.

Figure S3.



Supporting information, figure S3. Amplification factors for primary seismic sources. The effective bottom slope s defined by eq. (S22, Supporting information text) is shown for different bottom depth profiles and for frequencies ranging from 5 to 100 mHz. These estimates are median values over 11 contiguous depth profiles taken from (28-31). For the calculations shown in figures 1 and 2, we have used a constant $s = 6$. The exact location of east-west depth profiles are a 1 degree interval around 41° N (mid-Atlantic ridge), and 0.2° intervals around 46.47°N (Bay of Biscay), 41.473°N (Oregon shelf), and north-south profiles around 157.8°W across the Oahu north shore, Hawaii. The seismic source power is proportional to s .

Figure S4.



Supporting information, figure S4. Primary seismic sources over the mid-Atlantic ridge. Results for 100 s infragravity waves over a depth profile taken from the mid-Atlantic ridge, north of the Azores, at 41°N. **a**, Bottom topography, **b**, bottom pressure computed using linear wave theory and energy conservation. **c**, seismic source power due to waves between the local position x and $x=1500$ km, estimated from the variance of the spatially-averaged bottom pressure.